Available online at www.sciencedirect.com
ScienceDirect
Journal of Solid State Chemistry 180 (2007) 2950–2957
JOURNAL OF SOLID STATE CHEMISTRY
www.elsevier.com/locate/jssc

Self-assembled multilayer films of poor water-soluble copper(II) complexes constructed from dipyrido[3,2-*d*:2′,3′-*f*]quinoxaline (Dpq) ligand as well as their fluorescent properties

Xiuli Wang*, Jiani Fang, Yanfeng Bi, Haiyan Zhao, Baokuan Chen, Hongyan Lin, Guocheng Liu

Faculty of Chemistry and Chemical Engineering, Bohai University, Jinzhou 121000, PR China

Received 4 June 2007; received in revised form 17 July 2007; accepted 27 July 2007
Available online 6 September 2007

Abstract

New multilayer films were prepared by alternating adsorption of poly(sodium 4-styrenesulfonate) (PSS) and a new complex of $[Cu_2(Dpq)_2(Ac)_2(H_2O)_2]$ $(ClO_4)_2 \cdot H_2O$ (**1**) (Dpq = dipyrido[3,2-*d*:2′,3′-*f*]quinoxaline, Ac = acetate) or a related complex $[Cu(Dpq)_2(H_2O)]$ $(ClO_4)_2 \cdot H_2O$ (**1a**) by electrostatic layer-by-layer self-assembly technique, respectively. Compounds **1** and **1a** have been synthesized and structurally characterized by elemental analyses, IR spectroscopy, and single-crystal X-ray diffraction analyses. Single-crystal X-ray analyses show that complexes **1** and **1a** possess a dinuclear and a mononuclear structure, respectively, which are further extended into layered frameworks by π–π stacking and hydrogen-bonding interactions. The multilayer films were characterized by UV–vis spectroscopy, fluorescence spectroscopy, small-angle X-ray reflectivity measurements, and atomic force microscopy (AFM) imaging. UV spectroscopy shows that the deposition process is regular and highly reproducible from layer to layer. AFM image indicates that the film surface is uniform and smooth. The fluorescent properties of the films were studied and the results showed that the forming condition of the films had great influence on their properties.

Keywords: Layer-by-layer self-assembly; Film; Copper(II) complex; Crystal structure; Fluorescence property

1. Introduction

In recent years, self-assembled multilayer films technique has drawn increasing attention in material science for fundamental research and intensive applications in the fields of composites, catalysis, biomaterials, microelectronics, nonlinear optics, sensor, and so on [1–4]. The layer-by-layer (LBL) self-assembled technique was applied to produce multilayer films reported first by Iler in 1966 and developed by Decher and Hong in the early 1990s [5–7]. Since then this LBL technique has been a premier approach because of its simplicity and versatility [8]. LBL films are predominantly assembled by the alternate deposition of oppositely charged species onto a charged solid surface, where electrostatic forces facilitate layer build-up [9,10]. As such, a broad scope of materials can be incorporated into the multilayer films with precision including synthetic polymers, fluorescent dyes, charged nanoparticles, and biological macromolecules [11–14]. Most of materials which can be assembled into multilayer films by LBL methods are water-soluble. More recently, there also have been several reports about some water-insoluble or poor water-soluble polymers can be assembled into multilayer films by LBL methods on the basis of hydrogen bond, coordination bond, or charge-transfer interaction [15–17]. But it is still difficult to incorporate the water-insoluble or poor water-soluble complex into the multilayer films by LBL electrostatic interaction [18].

The fact that coordination compounds have attracted increasing attention not only stems from their fascinating structures but also from their potential applications as new materials [19]. Meanwhile, copper-containing complexes are an important class of materials in view of their growing

*Corresponding author. Fax: +86 416 3400158.
E-mail address: wangxiuli@bhu.edu.cn (X. Wang).

0022-4596/$ - see front matter © 2007 Elsevier Inc. All rights reserved.
doi:10.1016/j.jssc.2007.07.033

significance, for example, as porous solids, sensors, molecular magnets, optical materials, and in supramolecular chemistry and catalysis [20]. However, most of the coordination compounds are water-insoluble or poor water-soluble, which may limit their applications. Based on above considerations, incorporating these complexes into multilayer films by LBL self-assembly method could be helpful in a wide range of applications.

Herein, our group purposefully designed and synthesized a new charged poor water-soluble dinuclear copper(II) complex $[Cu_2(Dpq)_2(Ac)_2(H_2O)_2]$ $(ClO_4)_2 \cdot H_2O$ (**1**) (Dpq = dipyrido[3,2-*d*:2′,3′-*f*]quinoxaline, Ac = acetate) and a related mononuclear copper(II) complex $[Cu(Dpq)_2(H_2O)]$ $(ClO_4)_2 \cdot H_2O$ (**1a**) [21], which might be used as new fluorescence materials, and subsequently were incorporated into mutilayer films by LBL methods. Compounds **1** and **1a** have been structurally characterized by elemental analyses, IR spectroscopy, and single-crystal X-ray diffraction analyses. The film growth was monitored by UV–vis spectroscopy and the surface morphology of the films was observed by atomic force microscopy (AFM). The film structure was characterized by X-ray reflectivity (XRR) measurements, and the fluorescent properties of these multilayer films were also investigated by fluorescence spectroscopy.

2. Experimental

2.1. Materials

Dpq was synthesized by the method of the literature [22]. Poly(sodium 4-styrenesulfonate) (PSS), MW 70000; poly(allylamine hydrochloride) (PAH), MW 70000; and poly(ethyleneimine) (PEI), MW 50000 were purchased from Aldrich. The water used in all experiments was deionized to a resistivity of 17–18 MΩ cm. All other chemicals purchased were of reagent grade and used without further purification.

The PSS/Cu^{II} complex multilayer films were deposited onto the following solid substrates for detailed characterization: quartz slides for UV–vis absorption, fluorescence, XRR, and single-crystal silicon wafers for AFM. All solid substrates were cleaned with piranha solution (H_2O_2:H_2SO_4 = 3:7 v/v) at 80 °C for 1 h, followed by thorough rinsing with deionized water. Further purification was carried out by immersion of the substrates in NH_4OH:H_2O_2:H_2O (1:1:5 v/v) solution at 70 °C for 30 min and then extensively washing with water and drying with N_2. The cleaned substrates were hydrophilic and stored in deionized water prior to use [23].

2.2. Characterization

FT-IR spectra (KBr pellets) were taken on a Magna FT-IR 560 spectrometer and ^1H NMR analyses were performed on a Varian Mercury V × 300 spectrometer Analyzer. UV–vis absorption spectra were recorded on a quartz slide using a UV-2550 spectrophotometer. Fluorescence spectra were performed on a Hitachi F-4500 fluorescence spectrophotometer at room temperature. XRR experiments were performed with a Philips X'Pert instrument using Cu*K*α radiation (λ = 1.5405 Å). AFM images were obtained in a commercial microscope (AJ-III Scanning Probe Microscope, Shanghai AJ Nano-Science Development Co. Ltd.) by tapping mode with pyramidal tips and cantilevers made from etched silicon probes.

2.3. General synthetic procedure

2.3.1. Synthesis of complex $[Cu_2(Dpq)_2(Ac)_2(H_2O)_2]$ $(ClO_4)_2 \cdot H_2O$ (1)

A mixture of $Cu(ClO_4)_2 \cdot 6H_2O$ (0.027 g, 0.1 mmol) and Dpq (0.024 g, 0.1 mmol) with 5 mL acetic acid and 5 mL ethanol was stirred for 20 min, then transferred and sealed in a 25 mL teflon-lined stainless-steel container, which was heated to 120 °C for 48 h and cooled to room temperature at a rate of 5 °C/h. Blue block crystals were obtained and washed by water and ethanol, and dried in air. Yield: 85% (based on Cu). Calcd. for $C_{32}H_{26}Cl_2Cu_2N_8O_{14}$: C 40.6, H 2.7, N 11.8%; found: C 40.7, H 2.8, N 11.9%. IR (KBr) *v*: 3465 (m), 1579 (w), 1487 (s), 1431 (w), 1087 (w), 823 (s), 731 (s), 647 (m).

2.3.2. Synthesis of complex $[Cu(Dpq)_2(H_2O)]$ $(ClO_4)_2 \cdot H_2O$ (1a)

A mixture of $Cu(ClO_4)_2 \cdot 6H_2O$ (0.027 g, 0.1 mmol), and Dpq (0.024 g, 0.1 mmol) with 5 mL acetic acid and 5 mL acetonitrile was stirred for 2 h. The resulting solutions were filtered and the filtrates were allowed to stand in air at room temperature for several days, yielding green block crystals of **1a**. Yield: 74% (based on Cu). Calcd. for $C_{28}H_{20}Cl_2CuN_8O_{10}$: C 44.1, H 2.6, N 14.7%; found: C 44.1, H 2.8, N 14.6%. IR (KBr) *v*: 3120 (w), 1588 (m), 1480 (s), 1409 (s), 1385 (s), 823 (s), 724 (s), 617 (s).

2.3.3. X-ray crystallography

Crystallographic data for **1** was collected at 293(2) K on a Bruker Smart 1000 CCD diffractometer with Mo*K*α (λ = 0.71073 Å) by ω scan mode. All the structures were solved by direct methods using the SHELXS program of the SHELXTL package and refined by full-matrix least-squares methods with SHELXL [24,25]. Hydrogen atoms of the ligand were generated theoretically onto specific atoms and refined isotropically with fixed thermal factors. Crystal data for **1**: M = 944.61, Monoclinic, Pc, a = 8.703(2) Å, b = 18.517(4) Å, c = 11.836(3) Å, β = 108.980(4)°, V = 1803.7(7) $Å^3$, Z = 2, Dc = 1.739 g cm^{-3}, μ = 1.410 mm^{-1}, $F(0\,0\,0)$ = 956.0, R = 0.0552 and wR_2 = 0.1260 for 3345 independent reflections with $[I > 2\sigma(I)]$. Crystal data for **1a** is listed in Table S1. Selected bond lengths and angles for **1** are presented in Table S2. Hydrogen-bonding geometries for **1** and **1a** are summarized in Table S3, respectively.

2.4. Film preparation

The following solutions were used to prepare PSS/Cu^{II} complex multilayer films (**1**–**4**): Aqueous PEI solution (5 mg mL^{-1}), aqueous PSS solution (2 mg mL^{-1} and containing 0.5 mol L^{-1} NaCl), aqueous PAH solution (2 mg mL^{-1} and containing 0.5 mol L^{-1} NaCl), and DMF:H_2O = 1:1(v:v) Cu^{II} complex solution (10^{-3} mol L^{-1}).

The fabrication of the multilayer films (**1**–**4**) was carried out according to the following steps. At first, a PEI/PSS/PAH precursor (**P**) film was deposited onto a cleaned substrate (quartz, silicon) by immersing the substrate alternately in PEI, PSS, and PAH solutions for 20 min each, followed by rinsing with deionized water and drying in nitrogen after each immersion. Then the substrate-supported precursor (**P**) film was alternately dipped into the PSS and the Cu^{II} complex solutions for 20 min, rinsed with deionized water and dried in a nitrogen stream after each dipping, respectively. It should be noted that Cu^{II} complex solutions for multilayer films **1** and **3** were used soon after Cu^{II} complexes were dissolved in DMF–H_2O, while solutions for multilayer films **2** and **4** were allowed to stand at room temperature for 24 h, respectively. This process can be repeated until the desired number of bilayers is obtained. All adsorption procedures were performed at room temperature. The multilayer architectures thus obtained can be expressed as **P**/(PSS/Cu_2–Dpq)$_n$ (for films **1** and **2**) and **P**/(PSS/Cu–Dpq)$_n$ (for films **3** and **4**), respectively.

3. Results and discussion

3.1. Description of crystal structure

3.1.1. $[Cu_2(Dpq)_2(Ac)_2(H_2O)_2]\ (ClO_4)_2 \cdot H_2O$ (**1**)

Single-crystal X-ray analysis reveals that complex **1** is a unique 2-D double-layered supramolecular framework in which the asymmetric unit contains two Cu(II) ions. Each of the Cu(II) ions is coordinated by two oxygen atoms from two distinct acetate ligands with Cu–O bond distances ranging from 1.927(7) to 1.974(6) Å, two nitrogen atoms from one Dpq ligand (average Cu–N distance 2.073 Å), and a coordinated H_2O molecule, showing distorted tetragonal–pyramidal coordination geometry. The two Cu(II) ions are bridged by two acetate ligands

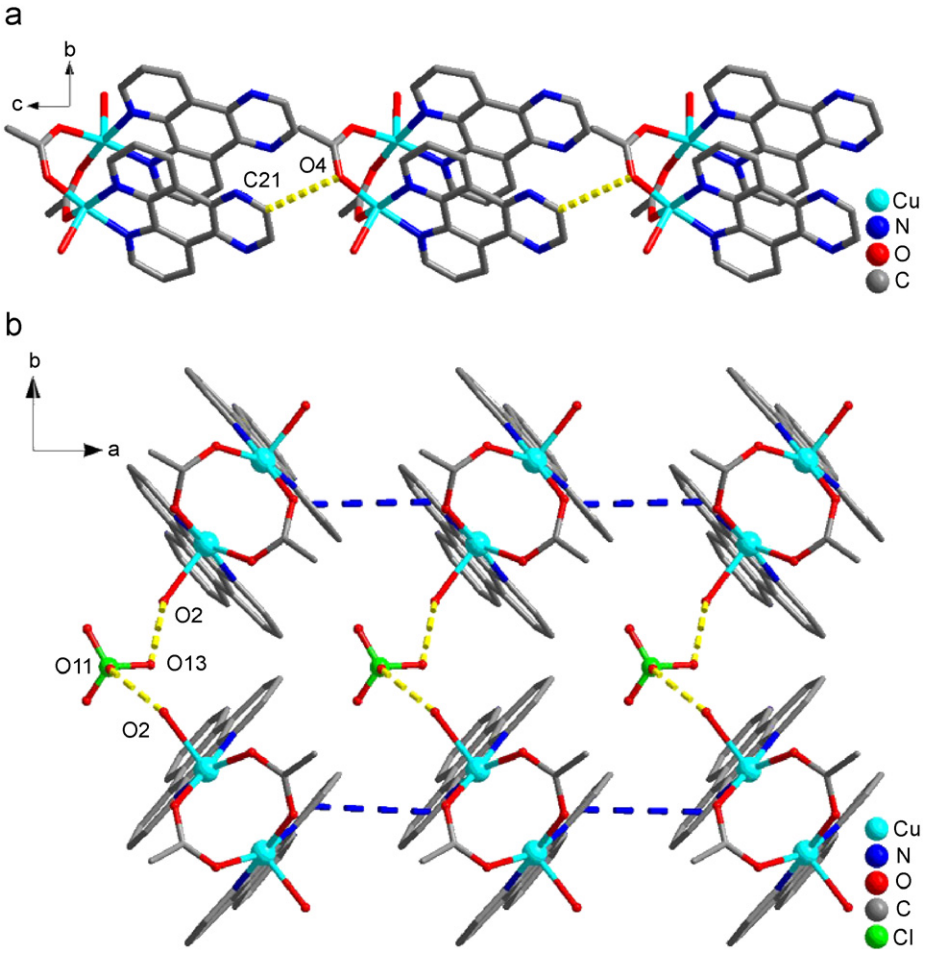

Fig. 1. (a) 1-D chain-like supramolecular network of **1** formed by C–H···O bonds and (b) the double-layered supramolecular structure stacked by π–π stacking interactions and strong hydrogen bond chains (part of H atoms and ClO_4^- are omitted for clarity).

to form a dinuclear unit with Cu···Cu distance ca. 3.06 Å (see Fig. S1).

Additionally, the dinuclear units are linked by hydrogen bonds between the hydrogen atoms [C(21)–H(21A)] from Dpq ligands and the oxygen atoms O(4) of acetate [C(21)–H(21A)···O(4), 3.38 Å, 161°] into 1-D chain viewed along *a*-axis (Fig. 1a). Furthermore, along the *c*-axis direction, the 1-D chains are ultimately extended into a 2-D double-layered supramolecular structure through π–π stacking interactions between aromatic groups of Dpq ligands (face-to-face distance ca. 3.01 Å) and hydrogen bond chains O(2)–O(13)–Cl(2)–O(11)–O(2) as shown in Fig. 1b.

3.1.2. $[Cu(Dpq)_2(H_2O)](ClO_4)_2 \cdot H_2O$ (**1a**) [21]

Single-crystal X-ray analysis reveals that complex **1a** is a mononuclear structure, which is stacked into a double-chain supramolecular structure through π–π stacking interactions between aromatic groups of Dpq ligands (face-to-face distance ca. 3.46 Å) and strong hydrogen bond chains O(9)–O(W)–Cl(1)–O(3)–O(9) (see Fig. S2).

3.2. UV–vis spectra of the films

The growth process of multilayer films containing Cu^{II} complexes was investigated by means of UV–vis spectra. Fig. 2 shows the UV absorbance spectra of four **P**/(PSS/Cu^{II} complexes)$_n$ ($n = 0$–7) multilayer films (**1**–**4**) assembled with the following order: Fig. 2a and b show the UV–vis spectra of **P**/(PSS/Cu_2–Dpq)$_n$ multilayer films **1** and **2**, respectively. The UV–vis spectra of **P**/(PSS/Cu–Dpq)$_n$ multilayer films **3** and **4** are depicted in Fig. 2c and d, respectively.

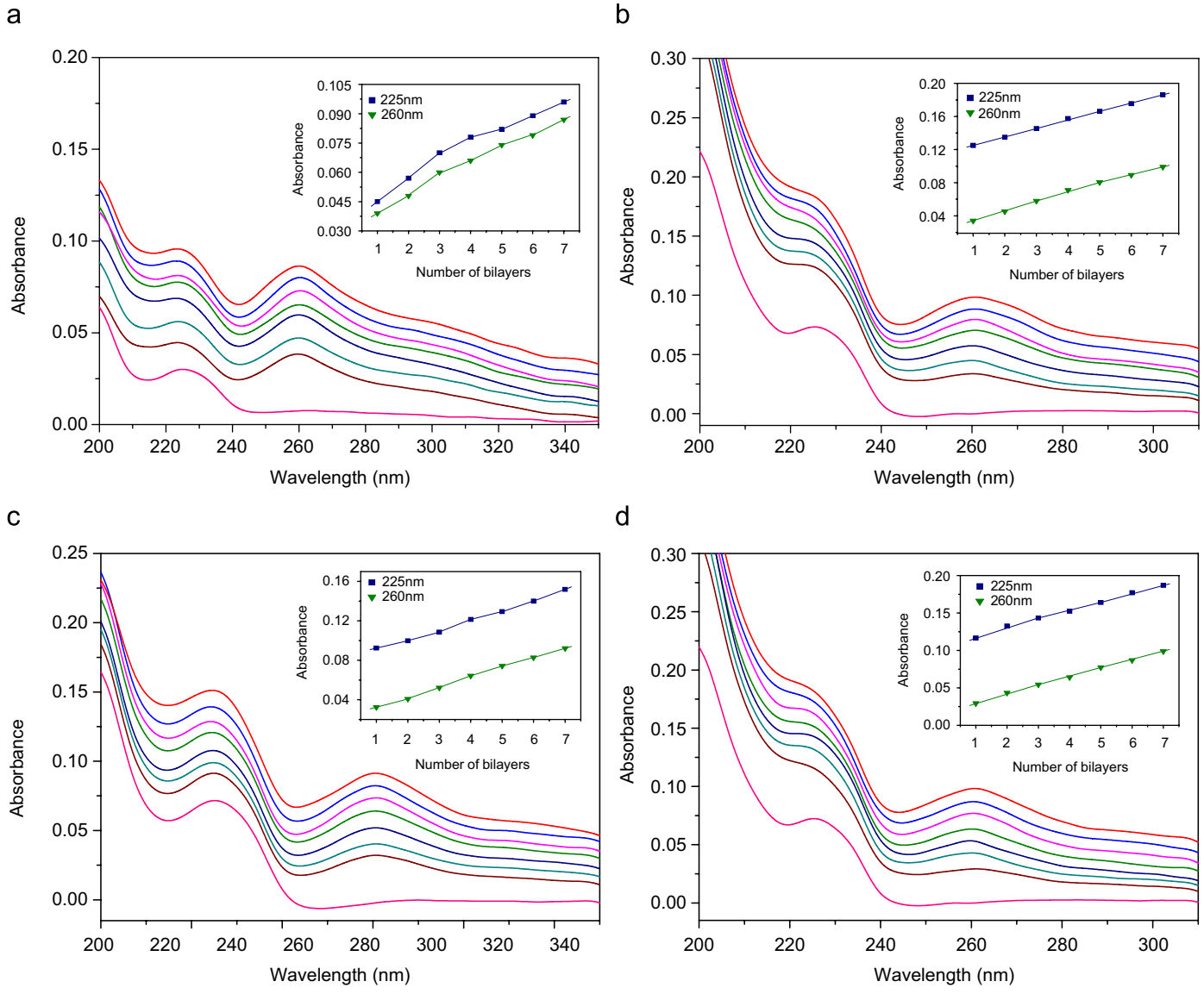

Fig. 2. UV–vis adsorption spectra of (a) films **1**, (b) films **2**, (c) films **3**, and (d) films **4**, respectively. The lowest curve corresponds to the precursor (**P**) film ($n = 0$). The insets show plots of the absorbance values at 225 and 260 nm as a function of the number of PSS/Cu^{II} complexes bilayers.

Since PEI and PAH does not absorb above 200 nm, the absorption band at 225 nm is due to the benzene ring of PSS molecules in the precursor (**P**) film with $n = 0$ [26]. The films exhibit the characteristic bands of the Cu^{II} complexes **1** and **1a** at 260 nm, which confirms the incorporation of Cu^{II} complexes into multilayer films. The insets in Fig. 2 present the plots of the absorbance values for these multilayer films at 225 and 260 nm as a function of the number of deposition cycles. It can be seen that the linearity of films **2** and **4** (the insets of Fig. 2b and d) is better than that of films **1** and **3** (the insets of Fig. 2a and c), which indicates that films **2** and **4** exhibit more homogeneous multilayer growth than that of films **1** and **3** [27]. It is possible to precisely control the amount of fluorescence materials deposited simply by controlling the bilayer number.

However, it is interesting to note that the absorbance value corresponding to the deposition of the first (PSS/Cu^{II} complexes) bilayer onto the precursor (**P**) film is larger than that of the later bilayer, indicating that a greater amount of the Cu^{II} complex penetrated the precursor (**P**) film [28].

The influence of concentration of Cu complex solutions on the multilayer assembly was investigated. Regular (or approximately regular) growth was observed in a wide range of the concentrations of Cu complex solutions (from 10^{-5} to 10^{-2} mol L^{-1}), which confirms that the LBL self-assembly technique is also applicable to the fabrication of multilayer films of poor water-soluble Cu complex. In addition, the absorbance increased almost in proportion with the Cu complex concentrations (from 10^{-5} to 10^{-2} mol L^{-1}). When the Cu complex concentration is higher than 10^{-3} mol L^{-1}, the absorbance increases slightly, suggesting that the adsorption of Cu complex tends to saturation.

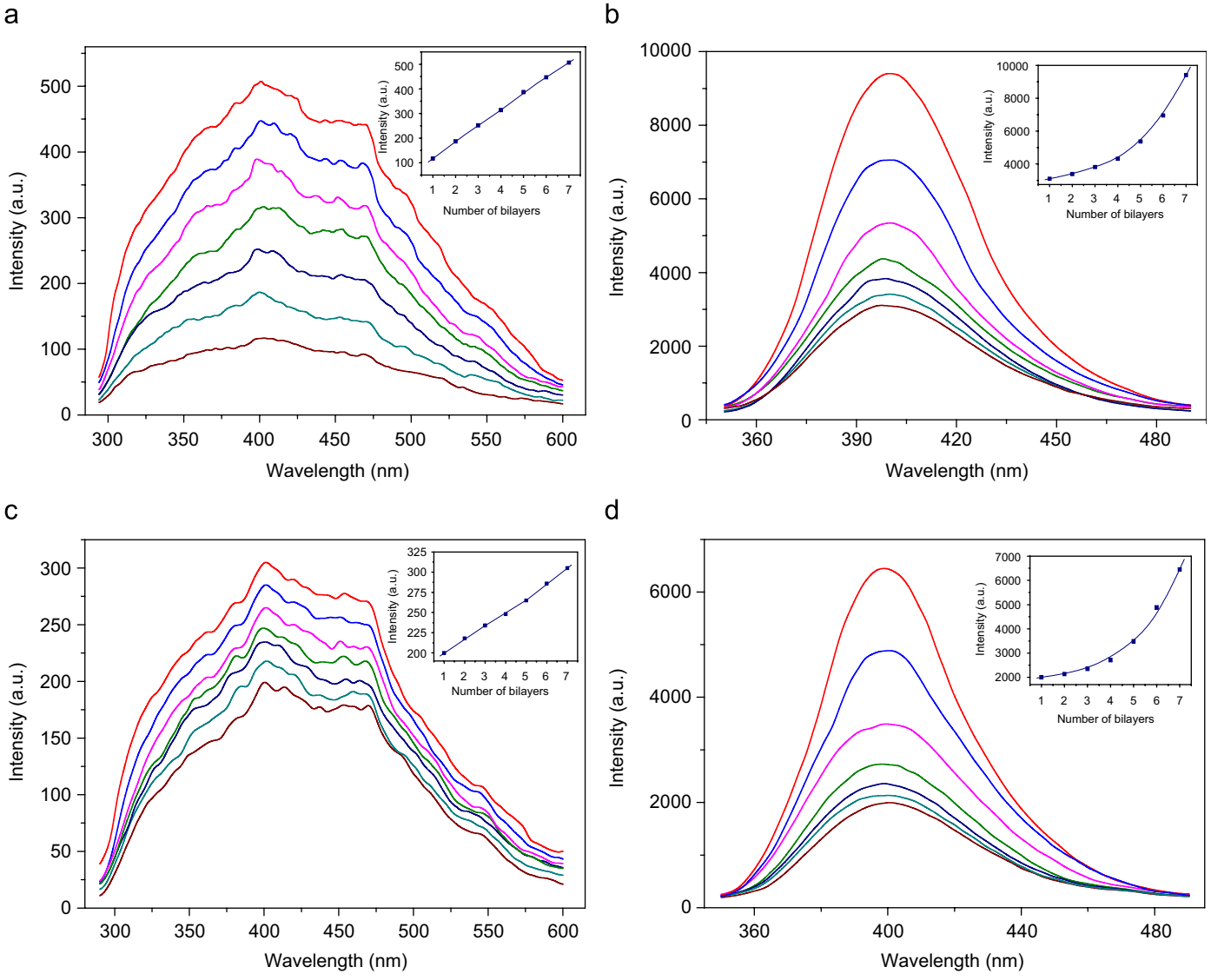

Fig. 3. Fluorescence emission spectra of (a) films **1**, (b) films **2**, (c) films **3**, and (d) films **4**, respectively. The insets show the intensity growth at 400 nm as a function of the number of bilayers ($\lambda_{ex} = 255$ nm).

3.3. Fluorescence properties of the films

The fluorescence properties of the two compounds (**1** and **1a**) and the (PSS/Cu^{II} complexes)$_n$ ($n = 1$–7) multilayer films have been investigated at room temperature. The fluorescence spectra of compounds **1** and **1a** in the solid state exhibit the characteristic fluorescence emission peak at ca. 352, 400 and 471 nm upon excitation at 255 nm, respectively (see Fig. S3). The multilayer films **1** exhibit emission peaks at ca. 352, 400 and 471 nm upon excitation at 255 nm as shown in Fig. 3a, which is consistent with those of the solid compound. But the fluorescent intensity located at 400 nm increased, which could be assigned to the isolated dinuclear contribution of compound **1**, while two shoulder peaks at 352 and 471 nm could be due to the contribution of the different aggregated states of multi-dinuclear clusters formed by hydrogen bonds and π–π interactions as described in the crystal structure [29]. That is to say, compound **1** existed in multilayer films **1** in two forms: isolated dinuclear and multi-dinuclear clusters. Interestingly, the emission peak at 400 nm remarkably increased while the two shoulder peaks completely disappeared as shown in Fig. 3b, which indicated that only the isolated dinuclear units of compound **1** existed in films **2**. As reported [30], because of the long standing time in DMF–H_2O solution, the π–π interactions of multi-dinuclear clusters could be destroyed by polar DMF–H_2O solution, which makes the embedded Cu_2–Dpq multilayers exist in an isolated dinuclear unit form. Consequently such an isolated dinuclear unit in multilayers avoids the self-quenching of intra-clusters [31] and effectively increases the rigidity of the film surfaces, and thus makes the fluorescent intensity to significantly increase when compared to that of films **1**. That is to say, the different forming conditions of these films may result in their different fluorescence properties.

It can be seen from the inset of Fig. 3a that the variation of the fluorescent intensity with the number of PSS/Cu_2–Dpq bilayers of films **1** tends to increase almost linearly. Comparatively, as shown in inset of Fig. 3b, it is amazing that the fluorescence emission peak of films **2** at 400 nm yields an approximately exponential relationship.

Despite the different geometries and ligand environments of the two compounds, the fluorescence properties of films **3** and **4** (see Fig. 3c and d) are similar to that of films **1** and **2** in the peak profiles, except that the intensity is weaker than that of films **1** and **2**, respectively. The fluorescence emission peak of films **3** and **4** at 400 nm would be attributed to the isolated mononuclear unit as proved above by crystal structure of **1a**. These observations indicate that these materials may be excellent candidates for potential photoluminescence materials because of their remarkable fluorescence properties.

3.4. XRR measurements

Small-angle XRR was used to investigate the film structure. Fig. 4 shows the XRR curves for the multilayer films **P**/(PSS/Cu^{II} complexes)$_n$ ($n = 5$). The X-ray curves of the multilayer films are considered to be a series of Kiessig fringes, which results from X-ray interferences from the subtrate–film and film–air interfaces, suggesting that the film surfaces are moderately uniform and smooth. The absence of Bragg peaks in XRR curves indicates the absence of a lattice-like layer structure and points to entanglement between the layers. The total thickness of the films were calculated to be about 11.5, 10, 16.9, and 11.6 nm for films **1**–**4**, respectively, from the spacing of the Kiessig fringes [32]. The thickness of the precursor PEI/PSS/PAH film was calculated to be about 5 nm (Fig. S5 shows the XRR curves for the **P** film). Based on the above-mentioned date, therefore, we infer the average thickness of one bilayer to be about 1.3, 1.0, 2.4, and 1.3 nm, respectively. The thickness of films **1**, **3** are higher than that of films **2**, **4**, respectively, which may be due to the different existence of Cu complexes on films as described in the studies of fluorescence properties.

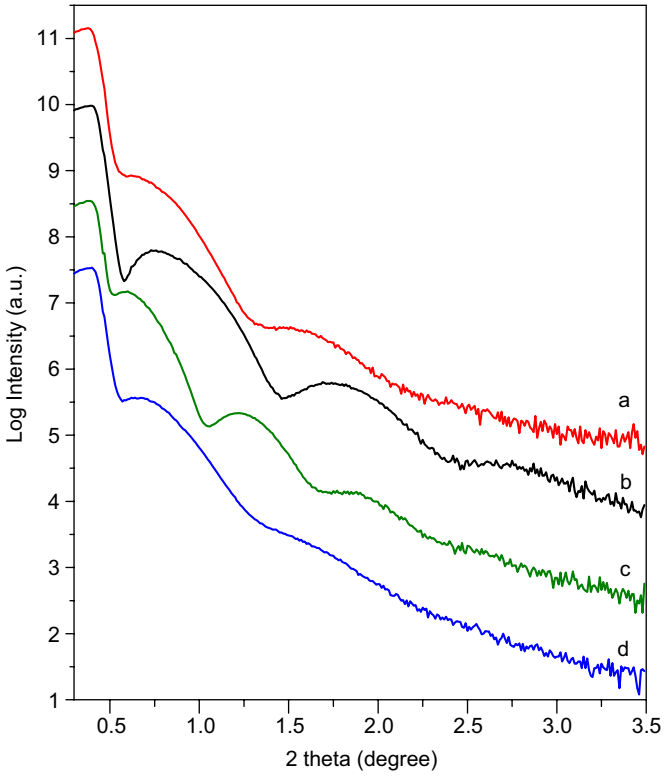

Fig. 4. X-ray reflectivity profiles of **P**/(PSS/Cu_2–Dpq)$_5$ (*a*) films **1**, (b) films **2** and **P**/(PSS/Cu–Dpq)$_5$, (c) films **3**, and (d) films **4**, respectively.

3.5. AFM images of the films

The AFM images of the (PSS/Cu^{II} complexes)$_n$ ($n = 5$) multilayer films (Cu^{II} complexes as the outermost layer) were taken to provide detailed information about the surface morphology and the homogeneity of the deposited films. Fig. 5a and b displayed an AFM image of the surface of the **P**/(PSS/Cu_2–Dpq)$_5$ multilayer films **1** and **2** on a single-crystal silicon substrate and Fig. 5c and d showed that of the **P**/(PSS/Cu–Dpq)$_5$ multilayer films **3** and **4**, respectively.

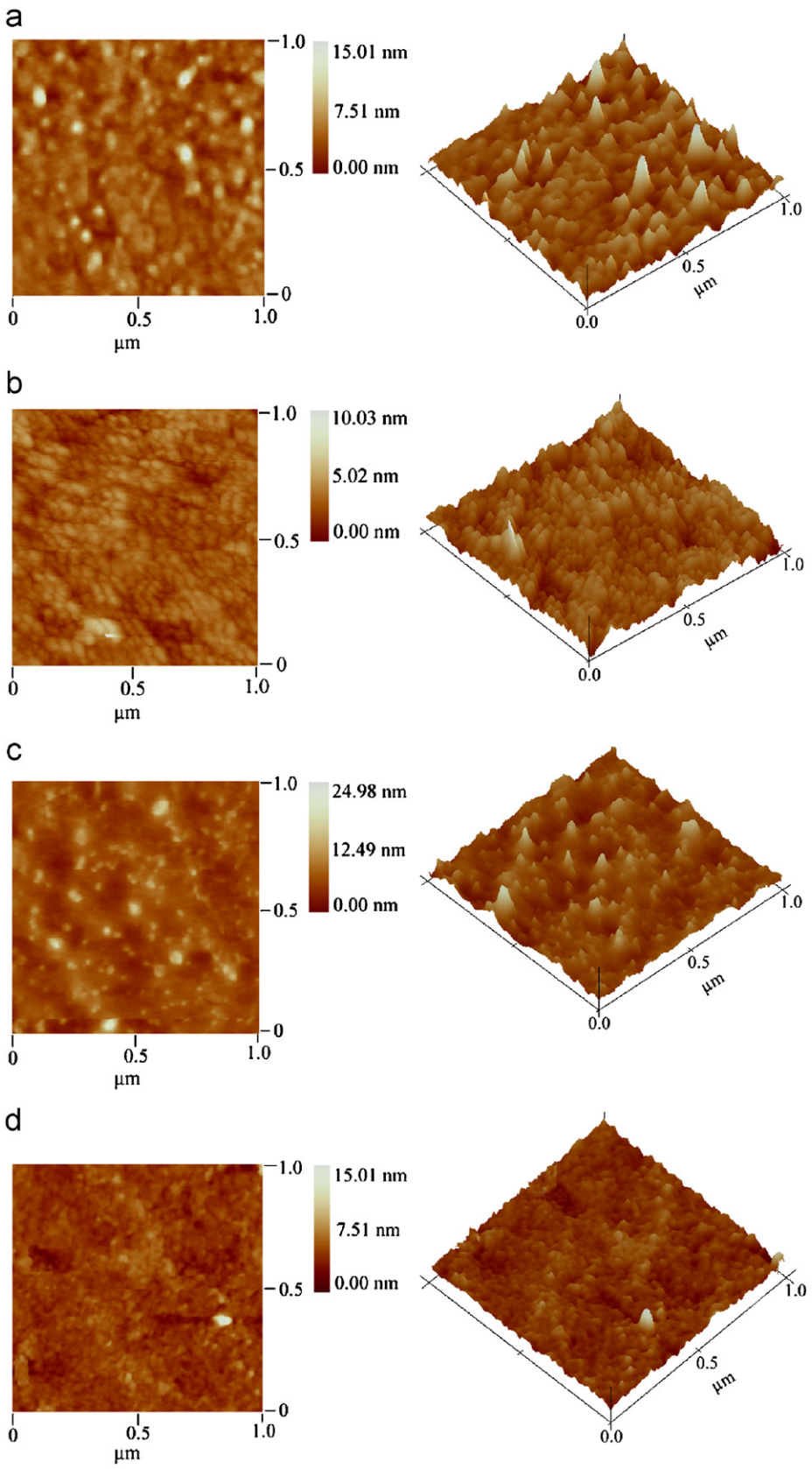

Fig. 5. AFM images of **P**/(PSS/Cu_2–Dpq)$_5$ (a) films **1**, (b) films **2** and **P**/(PSS/Cu–Dpq)$_5$, (c) films **3**, and (d) films **4**, respectively.

As can be seen, the surfaces of films **1** and **3** are made up of many spherical domains and some irregular blocks. The diameters of the spherical domains are approximately 15.8 and 14.7 nm along the horizontal axis, respectively. These domains are probably composed of complex ion pairs formed by the association of the Cu^{II} complex polycations with PSS polyelectrolyte chains via electrostatic interactions [33], and closely packed with each other and uniformly distributed in the whole films. The average diameters of irregular blocks are around 56.8 and 50.4 nm, respectively, which should be explained as an indirect reflection of aggregated multi-unit clusters Cu^{II} complex. The surface rms roughness over $1 \times 1\,\mu m^2$ is approximately 1.57 and 1.41 nm, respectively. The films **2** and **4**, however, show almost uniform and smooth surfaces with roughness of 1.01 and 1.04 nm, on which the spherical domains with a mean size of ca. 14.4 and 13.3 nm, respectively, and these domains are more closely packed with each other than that of films **1** and **3**. These differences can be attributed to the different existence form (multi-unit clusters and isolated units) of the complexes **1** and **1a** in the four films, which was consistent with the consequence of UV–vis, fluorescence spectra, and XRR measurements. This also provides the convincing evidence that the standing time of Cu^{II} complex solutions (used soon or left to stand at room temperature for 24 h after the Cu^{II} complexes were dissolved in DMF–H_2O) may have influence on film formation.

4. Conclusions

In this work, we synthesized a new dinuclear copper(II) complex **1** and a related mononuclear copper(II) complex **1a** and fabricated the highly ordered multilayer films (**1**–**4**) with these two complexes by LBL method, respectively. The films have been characterized by UV–vis spectroscopy, fluorescence spectroscopy, XRR measurements, and AFM imaging, which reveal both regular film growth and homogeneous surface morphology with Cu^{II} complex **1** and **1a**, respectively. The occurrence of fluorescence activity confirms the potential for creating photoluminescence multilayer films with the poor water-soluble complex. The significance of our work reveals the relationship between film forming conditions and film fluorescence properties of these complexes formed by hydrogen bonds and π–π interactions, that is, the change of film forming conditions have great influence on their properties.

Acknowledgment

The support of Natural Science Foundation of Liaoning Province (Grant 20061073) is gratefully acknowledged.

Appendix A. Supplementary materials

Crystallographic data (excluding structure factors) for the structure reported in this paper have been deposited with the Cambridge Crystallographic Data Centre as supplementary publication no. CCDC: 604934 (**1**). Copies of the data can be obtained free of charge on application to CCDC, 12 Union Road, Cambridge CB2 1EZ, UK (Fax: (44) 1223336-033; e-mail: deposit@ccdc.cam.ac.uk).

The online version of this article contains additional supplementary data. Please visit doi:10.1016/j.jssc.2007.07.033

References

[1] Z. Tang, Y. Wang, P. Podsiadlo, N.A. Kotov, Adv. Mater. 18 (2006) 3203.
[2] C. Jiang, V.V. Tsukruk, Adv. Mater. 18 (2006) 829.
[3] L. Xu, E.B. Wang, Z. Li, D.G. Kurth, X.G. Du, H.Y. Zhang, C. Qin, New J. Chem. 26 (2002) 782.
[4] A.G. Skirtach, B.G. De Geest, A. Mamedov, A.A. Antipov, N.A. Kotov, G.B. Sukhorukov, J. Mater. Chem. 17 (2007) 1050.
[5] R.K. Iler, J. Colloid Interface Sci. 21 (1996) 569.
[6] G. Decher, J.D. Hong, J. Schmitt, Macromol. Chem. Macromol. Symp. 46 (1991) 321.
[7] X. Zhang, H. Chen, H.Y. Zhang, Chem. Commun. (2007) 1395.
[8] A.P.R. Johnsto, H. Mitomo, E.S. Read, F. Caruso, Langmuir 22 (2006) 3251.
[9] G. Decher, Science 277 (1997) 1232.
[10] G. Decher, J.D. Hong, J. Schmitt, Thin Solid Films 210 (1992) 831.
[11] P. Bertrand, A. Jonas, A. Laschewsky, R. Legras, Macromol. Rapid Commun. 21 (2000) 319.
[12] W. Jin, X.Y. Shi, F. Caruso, J. Am. Chem. Soc. 123 (2001) 8121.
[13] F. Cui, J.H. Zhang, T.Y. Cui, K. Han, B. Xie, Q. Lin, B. Yang, Colloid Surf A 278 (2006) 39.
[14] H.Y. Ma, J. Peng, Y.H. Chen, Y.H. Feng, E.B. Wang, J. Solid State Chem. 177 (2004) 3333.
[15] H.M. Xiong, M.H. Cheng, Z. Zhou, X. Zhang, J.C. Shen, Adv. Mater. 10 (1998) 529.
[16] L.Y. Wang, Z.Q. Wang, X. Zhang, J.C. Shen, L.F. Chi, H. Fuchs, Macromol. Rapid Commun. 18 (1997) 509.
[17] Y. Shimazaki, M. Mitsuishi, S. Ito, M. Yamamoto, Langmuir 13 (1997) 1385.
[18] N. Ma, H.Y. Zhang, B. Song, Z.Q. Wang, X. Zhang, Chem. Mater. 17 (2005) 5065.
[19] B. Moulton, M.J. Zaworotko, Chem. Rev. 101 (2001) 1629.
[20] X.H. Bu, M.L. Tong, H.C. Chang, S. Kitagawa, S.R. Batten, Angew. Chem. Int. Ed. 43 (2004) 192.
[21] B.K. Santra, P.A.N. Reddy, G. Neelakanta, S. Mahadevan, M. Nethaji, A.R. Chakravarty, J. Inorg. Biochem. 89 (2002) 191.
[22] J.G. Collins, A.D. Sleeman, J.R. Aldrich–Wright, I. Greguric, T.W. Hambley, Inorg. Chem. 37 (1998) 3133.
[23] W. Kern, Semicond. Int. 7 (1984) 94.
[24] G.M. Sheldrick, SHELXS-97, Program for Crystal Structure Solution, University of Göttingen, Germany, 1997.
[25] G.M. Sheldrick, SHELXL-97, Program for Crystal Structure Refinement, University of Göttingen, Germany, 1997.
[26] F. Caruso, D.G. Kurth, D. Volkmer, M.J. Koop, A. Müller, Langmuir 14 (1998) 3462.
[27] Y.H. Wang, C.W. Hu, Thin Solid Films 476 (2005) 84.
[28] M. Jiang, E.B. Wang, G. Wei, L. Xu, Z. Li, J. Colloid Interface Sci. 275 (2004) 596.
[29] J. Lang, M.H. Liu, J. Phys. Chem. B. 103 (1999) 11393.
[30] Y.H. Feng, J. Peng, Z.G. Han, H.Y. Ma, J. Colloid Interface Sci. 286 (2005) 589.
[31] K. Binnemans, P. Lenaerts, K. Driesen, C. Görller-Walrand, J. Mater. Chem. 14 (2004) 191.
[32] J. Schmitt, T. Grunewald, G. Decher, P.S. Pershan, K. Kjaer, M. Losche, Macromolecules 26 (1993) 7058.
[33] Y.H. Wang, X.L. Wang, C.W. Hu, J. Colloid Interface Sci. 249 (2002) 307.